Journal of Biomolecular NMR, 5 (1995) 110–121
ESCOM

J-Bio NMR 257

Solution structure of porcine pancreatic phospholipase A_2 complexed with micelles and a competitive inhibitor

B. van den Berg[a], M. Tessari[b], R. Boelens[b], R. Dijkman[a], R. Kaptein[b,*], G.H. de Haas[a] and H.M. Verheij[a]

[a]*Center for Biomembranes and Lipid Enzymology, Division of Enzymology and Protein Engineering, Utrecht University, 3584 CH Utrecht, The Netherlands*
[b]*Bijvoet Center for Biomolecular Research, Utrecht University, 3584 CH Utrecht, The Netherlands*

Received 18 November 1994
Accepted 15 December 1994

Keywords: Phospholipase A_2; Interfacial activation; Ternary complex; NMR structure

Summary

The three-dimensional structure of porcine pancreatic PLA_2 (PLA_2), present in a 40 kDa ternary complex with micelles and a competitive inhibitor, has been determined using multidimensional heteronuclear NMR spectroscopy. The structure of the protein (124 residues) is based on 1854 constraints, comprising 1792 distance and 62 ϕ torsion angle constraints. A total of 18 structures was calculated using a combined approach of distance geometry and restrained molecular dynamics. The atomic rms distribution about the mean coordinate positions for residues 1–62 and 72–124 is 0.75 ± 0.09 Å for the backbone atoms and 1.14 ± 0.10 Å for all atoms. The rms difference between the averaged minimized NMR structures of the free PLA_2 and PLA_2 in the ternary complex is 3.5 Å for the backbone atoms and 4.0 Å for all atoms. Large differences occur for the calcium-binding loop and the surface loop from residues 62 through 72. The most important difference is found for the first three residues of the N-terminal α-helix. Whereas free in solution Ala^1, Leu^2 and Trp^3 are disordered, with the α-amino group of Ala^1 pointing out into the solvent, in the ternary complex these residues have an α-helical conformation with the α-amino group buried inside the protein. As a consequence, the important conserved hydrogen bonding network which is also seen in the crystal structures is present only in the ternary complex, but not in free PLA_2. Thus, the NMR structure of the N-terminal region (as well as the calcium-binding loop and the surface loop) of PLA_2 in the ternary complex resembles that of the crystal structure. Comparison of the NMR structures of the free enzyme and the enzyme in the ternary complex indicates that conformational changes play a role in the interfacial activation of PLA_2.

Introduction

Phospholipase A_2 (PLA_2; EC 3.1.14) is a calcium-dependent lipolytic enzyme that stereospecifically cleaves the *sn*-2-acyl linkage of *sn*-3-phospholipids (Waite, 1987). Phospholipases A_2 occur both intra- and extracellularly, and are involved in a number of important cellular processes, such as the liberation of arachidonic acid from membrane phospholipids, which plays a key role in the biosynthesis of prostaglandins and other mediators of inflammation (Irvine, 1982; Seilhamer et al., 1989). The extracellular PLA_2s are widespread in nature (Van den Bosch, 1980); very rich sources are pancreatic tissues of mammals and snake and bee venoms (Waite, 1987). They are small (14 kDa) enzymes, with a high stability under denaturing conditions, caused by the presence of six or seven disulfide bridges. Over 90 primary structures have been determined (Waite, 1987). The crystal structures of a number of PLA_2s have been solved and show a remarkable similarity. A mechanism of catalysis has been proposed (Verheij et al., 1980; Scott et al., 1990).

The catalytic activities of PLA_2s on monomeric substrates are low, but increase tremendously on aggregated substrates. This phenomenon is called interfacial activation. A number of models have been proposed to explain the activation process. The substrate models have in

*To whom correspondence should be addressed.

common that they assume the enzyme to be structurally invariant, and that the activation is caused by the changed properties of the substrate at the lipid–water interface (Scott et al., 1990; Scott and Sigler, 1994). In contrast, the enzyme models suppose that conformational changes of the enzyme are responsible for the high activities on aggregated substrates (Verger and De Haas, 1976). From the crystal structures, which are very similar for various PLA_2s both free and complexed to inhibitors, it was concluded that conformational changes do not occur in PLA_2. In other words, the crystal structures seem to favour the substrate models as an explanation for the interfacial activation.

The high-resolution 3D solution structure of free porcine pancreatic PLA_2 has been determined by NMR, using doubly labeled [^{13}C,^{15}N]-PLA_2 (Van den Berg et al., manuscript submitted for publication). The structure shows significant deviations from the crystal structures. Free in solution the first three N-terminal residues are disordered, whereas in the crystal structure an α-helical conformation is present. In addition, an important conserved hydrogen bonding network linking the α-amino group to the active site is incomplete in the free enzyme, whereas in the crystal structures it is intact. The presence of this network could be the cause for the low catalytic activities on monomeric substrates. We have proposed that when the enzyme binds to micelles with subsequent binding of an inhibitor in the active site, the N-terminus and the active-site residues adopt a rigid conformation, leading to high catalytic activities on aggregated substrates.

In the present paper we describe the assignment of the ^1H, ^{13}C and ^{15}N resonances of PLA_2 in the ternary complex, composed of the enzyme bound to micelles with a strong competitive inhibitor present in the active site, using doubly ^{13}C,^{15}N-labeled protein. The 3D solution structure of the enzyme in this ternary complex was determined using NOE distance constraints supplemented with a limited number of dihedral angle constraints. To our knowledge, this is the first solution structure determination of a lipolytic enzyme complexed to a high-molecular-weight lipid aggregate. Comparison of the NMR structures of the free enzyme and that in the ternary complex indicates that conformational changes play a role in the mechanism of interfacial activation of PLA_2.

Materials and Methods

Synthesis of the phosphonate transition-state analogue

The synthesis of the phosphonate transition-state analogue used in the current study was performed in a similar way as described in the literature (Yuan and Gelb, 1988; M.H. Gelb, personal communication). The structure of the inhibitor, (*R*)-1-thio-octyl-2-heptylphosphonyl-1-deoxyglycero-3-phosphoglycol, is shown in Fig. 1.

Inhibitory power of the phosphonate transition-state analogue

The inhibitory power (Z) of the phosphonate analogue with porcine pancreatic PLA_2 was determined in the pH stat using a mixed micellar system consisting of 3 mM sodium-taurodeoxycholate and 3 mM 1,2-didodecanoyl-*sn*-glycero-3-phosphocholine as the substrate (De Haas et al., 1990), in a buffer containing 150 mM NaCl, 50 mM $CaCl_2$ and 5 mM NaAc, pH 5.0, at a temperature of 25 °C. Under these conditions all enzyme is present at the interface (data not shown), and its specific activity is approximately 20 U/mg.

Determination of the molecular size of the ternary complex

The size of the ternary complex was determined using a Sephadex G75 gel filtration column (Pharmacia), essentially as described by De Araujo et al. (1979). To this end the enzyme (0.2 mM) was dissolved in a 5 mM acetate buffer, pH 4.3, containing 150 mM NaCl and 50 mM $CaCl_2$. Dodecylphosphocholine (DPC) was added in an 80-fold excess to PLA_2 (16 mM). The molecular weight of the protein–lipid complex was determined in the presence and absence of the phosphonate inhibitor in the active site of the enzyme (added in a 10% molar excess to the enzyme). The column was equilibrated in buffer containing 1.5 mM DPC. The elution volume of the ternary complex was calibrated using several non-lipid binding proteins with known molecular size.

Sample preparation

The preparation of the uniformly (> 90%) doubly ^{13}C, ^{15}N-labeled and 10% ^{13}C-labeled PLA_2 has been described (Van den Berg et al., manuscript submitted for publication). The protein (3 mM) was lyophilized and dissolved in 450 µl of an H_2O solution (containing 7% D_2O), in the presence of 250 mM (83 molar equiv) fully deuterated dodecylphosphocholine (DPC; Cambridge Isotope Laboratories) and 3.3 mM of the phosphonate inhibitor. The protein concentration in the 10% ^{13}C-labeled PLA_2 sample was 1.5 mM in D_2O, in the presence of 120 mM deuterated DPC and 1.65 mM inhibitor. All samples contained 150 mM NaCl and 50 mM $CaCl_2$, at pH 4.30.

NMR spectroscopy

All NMR spectra were recorded in 93% H_2O/7% D_2O at 313 K on a Bruker AMX600 spectrometer, equipped with a three-channel NMR interface and a triple-resonance [^1H,^{15}N,^{13}C]-probe with an additional gradient coil. The assignment of the backbone resonances was accomplished by recording and analysis of 3D triple-resonance HNCO, HNCA (Ikura et al., 1990a,b; Kay et al., 1990), HNCOCA (Bax and Ikura, 1991) and HCACO (Kay et al., 1990) experiments in combination with a conventional ^{15}N-edited TOCSY-HSQC experiment. The assignment of the side chain resonances of the ternary complex was, using various ^{13}C-edited HCCH-TOCSY experiments (Bax

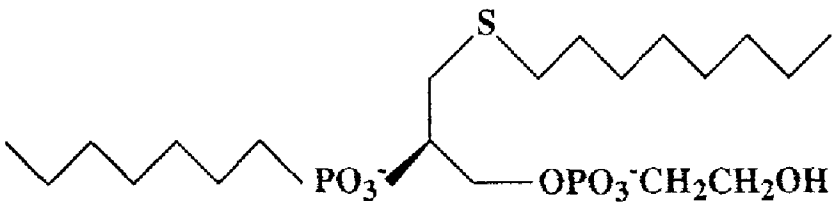

Fig. 1. Structure of the phosphonate transition-state analogue used in this study, (*R*)-1-thio-octyl-2-heptylphosphonyl-1-deoxyglycero-3-phosphoglycol.

et al., 1990a,b), carried out as described for the protein free in solution (Van den Berg et al., manuscript submitted for publication). The assignment of NOEs in the ternary complex was accomplished using a time-shared [^{15}N,^{13}C]-NOESY-HSQC experiment (Pascal et al., 1994; Vis et al., 1994), and a ^{13}C-edited NOESY-HSQC experiment for the aromatic region. The latter experiment was acquired with a mixing time of 100 ms, recording 100 complex points in F1 (^{1}H), 52 complex points in F2 (^{13}C) and 1024 complex points in F3. The spectral widths in the indirectly detected ^{1}H and ^{13}C dimensions were 5952 and 4000 Hz, with the carrier positions at 4.60 and 124.5 ppm. The spectral width in the ^{1}H acquisition dimension was 5952 Hz, with the carrier at the water frequency (4.60 ppm). The time-shared [^{15}N,^{13}C]-NOESY-HSQC experiment was acquired with a mixing time of 100 ms, recording 100 complex points in F1 (^{1}H), 48 complex points in F2 (^{15}N, ^{13}C) and 1024 complex points in F3. The spectral widths in the indirectly detected ^{1}H, ^{15}N and ^{13}C dimensions were 10 000, 2000 and 5000 Hz, with the carrier positions at 4.60, 117.5 and 39.7 ppm, respectively. The spectral width in the ^{1}H acquisition dimension was 10 000 Hz, with the carrier at the water frequency (4.60 ppm). All NMR spectra were processed on Silicon Graphics workstations using the in-house TRITON software package. Zero-filling (once or twice) was employed in all indirectly detected dimensions. Linear prediction was used in most cases to extend the data by approximately 30% in the heteronuclear dimensions. Separate baseline corrections were applied after the Fourier transformations and appropriate window function multiplications. The spectra were analysed directly on Silicon Graphics workstations using the program REGINE.

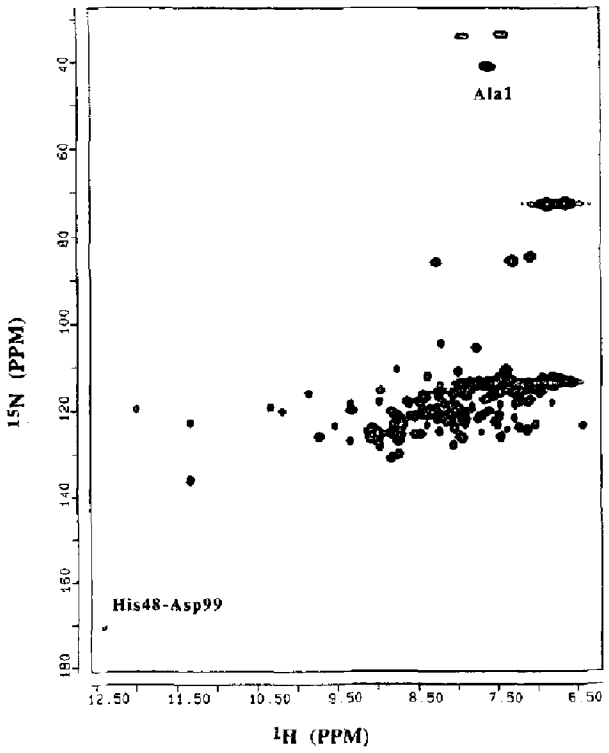

Fig. 2. [^{1}H,^{15}N]-HSQC spectrum of PLA_2 in the ternary complex. Note the resonance at 12.4/170.4 (^{1}H/^{15}N) ppm, which originates from the hydrogen bond between His^{48} and Asp^{99}, and the resonance at 7.61/40.9 ppm, which belongs to the α-ammonium group of Ala^{1}. The probable identity of the additional upfield ^{15}N signals is described in the text.

Stereospecific assignments

The stereospecific assignments for the prochiral methyl groups of the valine and leucine residues in PLA_2 were obtained from a [^{1}H,^{13}C]-HMQC spectrum recorded on a sample of 10% labeled enzyme present in the ternary complex (Senn et al., 1989). As with the protein free in solution, no stereospecific assignments for the prochiral α-protons of glycines and (β) methylene protons were used in the structure calculations.

Constraints

NOEs were assigned from 3D ^{13}C- and ^{15}N-edited NOESY spectra with mixing times of 100 ms. To relate the NOE intensities with distances we used the distances between δ- and ε-protons in aromatic residues (2.5 Å) and the $d_{\alpha N}(i,i+3)$ distances (3.5 Å) in α-helices as a calibration. The NOEs were classified as strong, medium, weak and very weak, corresponding to interproton distance constraints of 2.0–2.8, 2.0–3.7, 2.0–5.0 and 2.0–5.5 Å, respectively. The values of the pseudoatom corrections were 1.0, 0.9 and 2.0 Å, for methyl group protons, non-degenerate methylene protons and aromatic ring protons, respectively. Qualitative constraints for dihedral φ angles, obtained from a ^{15}N-HMQC-J experiment (Kay and Bax, 1989), were $-50 \pm 40°$ for $^{3}J_{HN\alpha} < 6$ Hz, and $-125 \pm 50°$ for $^{3}J_{HN\alpha} > 4$ Hz (Pardi et al., 1984). No hydrogen bonding constraints were used in the structure determinations,

and no constraints for calcium in the distance geometry calculations. However, because small changes in the structure of the calcium loop occurred during the refinement procedure, five constraints for the calcium ion, inferred from the crystal structure, were introduced during refinement. The corresponding calcium–ligand distances, involving the carboxyl oxygens of Asp^{49} and the backbone carbonyl oxygens of Tyr^{28}, Gly^{30} and Gly^{32}, were constrained between 3.0 and 4.0 Å (Dijkstra et al., 1983).

The final DG structures for PLA_2 in the ternary complex were calculated based on 1854 experimental NMR constraints, which is on average 15 constraints per residue. These constraints comprised 1792 approximate distances, which could be subdivided in the following way: 497 intraresidue, 593 sequential interresidue ($|i - j| = 1$), 365 medium-range ($2 \leq |i - j| \leq 5$), and 337 long-range ($|i - j| > 5$) constraints. In addition, 62 approximate ϕ torsion angle constraints were obtained.

Structure calculations

Protein structures were generated with distance geometry (Havel, 1991) using the DGII program (Biosym, San Diego, CA). An iterative procedure was used for the generation of the final structures, as described previously (Powers et al., 1993). The structures were refined with the program Discover (Biosym). The refinement protocol con-

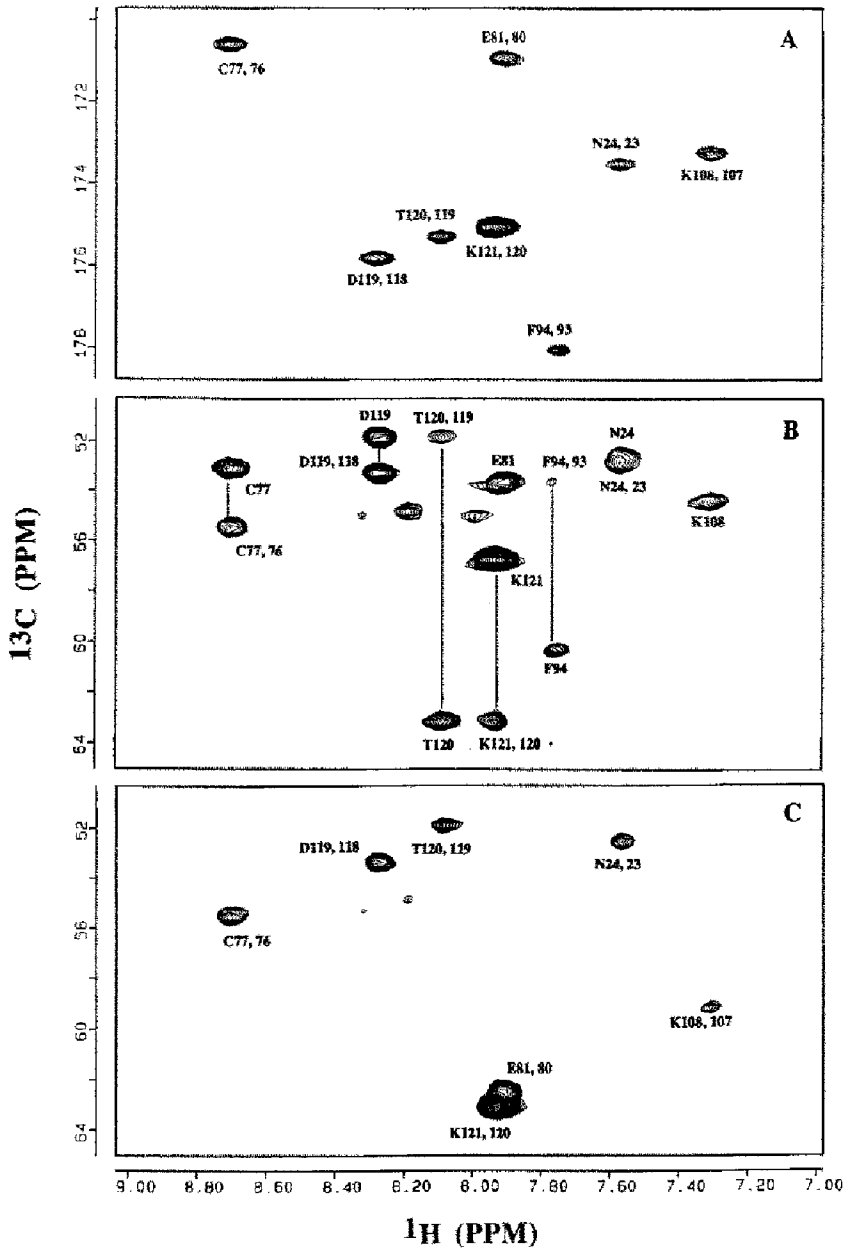

Fig. 3. Cross sections through ^1H-^{13}C planes of the HNCO (A), HNCA (B) and HNCOCA (C) triple-resonance spectra of PLA_2 in the ternary complex, taken at a ^{15}N chemical shift of 120.0 ppm. The intraresidual (HNCA) and interresidual (HNCA, HNCO, HNCOCA) connectivities from several amide resonances to the corresponding C^{α} or CO (HNCO) resonances are indicated.

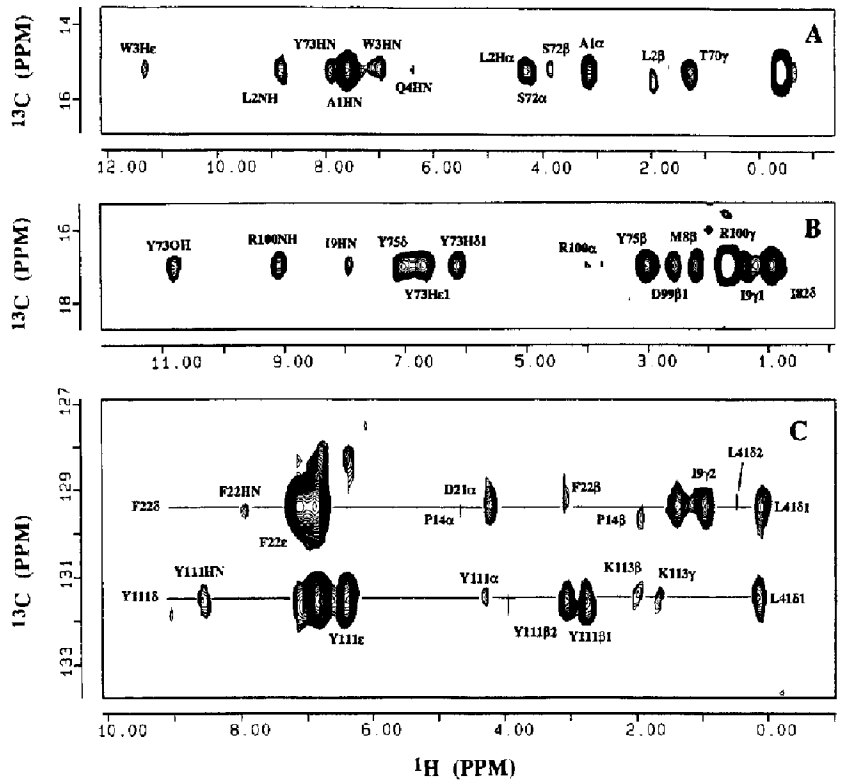

Fig. 4. Cross sections through the ^{1}H-^{13}C planes of the ^{13}C part of the time-shared [^{15}N,^{13}C]-NOESY spectrum and of the ^{13}C-edited NOESY spectrum in the aromatic region of PLA_2 in the ternary complex. The ^{1}H-^{13}C planes were taken at the ^{1}H chemical shift of the Ala^{1} β-proton at −0.36 ppm (A), the ε-CH_3 group of Met^{8} at 1.73 ppm (B), and the H^{δ} protons of Phe^{22} and Tyr^{111} at 6.80 ppm (C). Several long-range as well as short-range NOE contacts are indicated.

sisted of a restrained energy minimization step (100 iterations using steepest descent minimization and subsequently 1000 iterations using conjugate gradients minimization), followed by restrained molecular dynamics for 6 ps, using a consistent valence force field (CVFF; Biosym). Finally, another energy minimization step was performed (250 steepest descent steps, followed by 2000 conjugate gradients steps). Displaying and visual inspection of the structures was performed on Silicon Graphics workstations, using the InsightII program implemented in the NMRchitect software package (Biosym). The structures have been deposited in the Brookhaven protein databank.

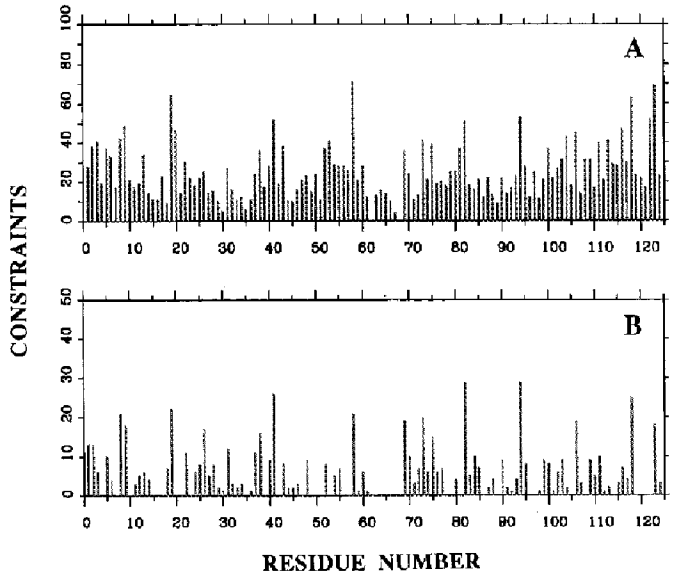

Fig. 5. Total number of NOE distance constraints (A) and number of long-range NOE distance constraints (B), assigned for PLA_2 in the ternary complex, shown as a function of the residue number.

Docking of the inhibitor in the active site of PLA_2 in the ternary complex

The phosphonate inhibitor was docked in the active site of the restrained minimized averaged NMR structure of PLA_2 in the ternary complex by performing a restrained energy minimization. In order to do this, a number of intermolecular NOEs were assigned from the heteronuclear 3D NOESY spectra, and distance constraints were generated in a similar way as for the intramolecular NOEs. The experimental NMR constraints were supplemented with two constraints inferred from the crystal structure. One constraint was introduced for the contact between the calcium ion and the phosphate group of the inhibitor. Another constraint was included for the contact of the Tyr^{69} hydroxyl group with the phosphate group of the inhibitor. In total, 16 intermolecular constraints between PLA_2 and the inhibitor were used. A list of the intermolecular protein–inhibitor contacts is included in the supplementary material to this paper.

Results and Discussion

Binding of the phosphonate inhibitor to PLA_2

The binding of a competitive inhibitor in the active site of PLA_2 can be expressed by means of the Z-value, which is – for strong inhibitors – proportional to the affinity of the enzyme for inhibitor over substrate (Ransac et al., 1990). At pH 5.0, a Z-value of 10 000 was obtained for the phosphonate analogue. Comparing this value to the Z-values for the acylamino substrate analogues used previously (ranging from 100 to 500 at pH 5.0; Dekker et al., 1991; Peters et al., 1992b), it is clear that under acidic pH conditions phosphonate transition-state analogues are much better inhibitors of PLA_2 than the corresponding acylamino analogues (Yu and Dennis, 1991).

The [^{1}H,^{15}N]-HSQC spectrum of the enzyme in the ternary complex with inhibitor and micelles at pH 4.3 is shown in Fig. 2. The spectrum shows cross peaks at 7.61/40.9 (^{1}H/^{15}N) and at 12.42/170.4 ppm, which were also observed in spectra obtained previously for the acylamino analogues at pH 5.0 (Peters et al., 1992a). These cross peaks originate from the α-amino group of Ala^1 and the important hydrogen bond between the side chains of the active-site residues His^{48} and Asp^{99}, respectively. In Fig. 2, two upfield ^{15}N resonances are visible close to the α-amino group resonance. The absence of these resonances in the spectrum of free PLA_2 could indicate that they are associated with the binding of the inhibitor in the active site of the enzyme. The ^{15}N-HSQC spectrum of the PLA_2 mutant K56M, in which Lys^{56} is replaced by a methionine, showed that the upfield ^{15}N signal at 7.93/33.9 ppm is likely to arise from an interaction between the Lys^{56} ζ-NH_3 group and the phosphoglycol headgroup of the inhibitor. This supports biochemical studies, from which

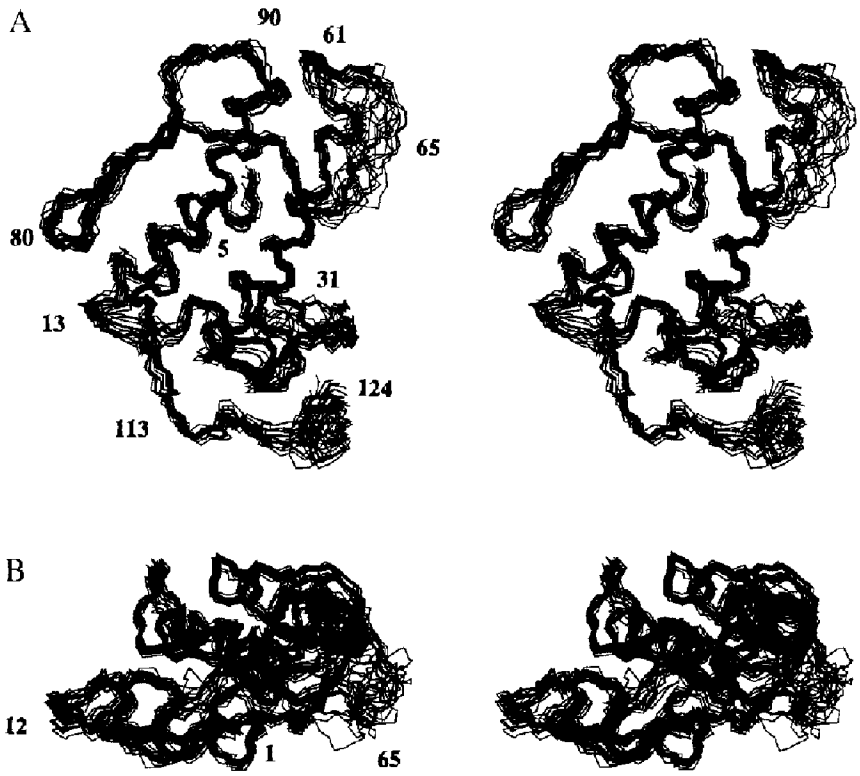

Fig. 6. Stereoviews showing the best fit superpositions of the backbone (N, C^α, CO) resonances of the 18 refined distance geometry structures of PLA_2 in the ternary complex. The view in (B) is rotated about the x-axis approximately 90° with respect to that in (A). The numbers of some amino acid residues are indicated.

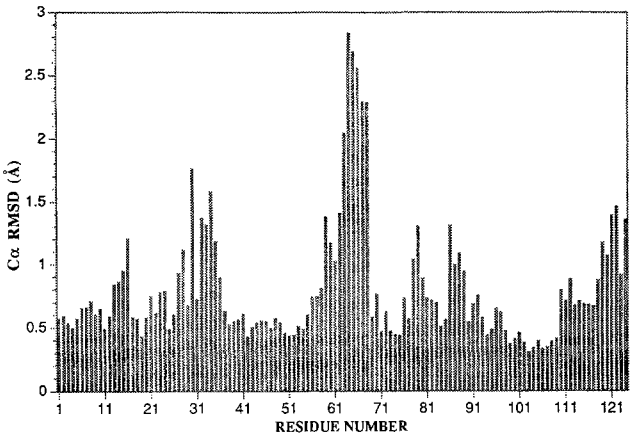

Fig. 7. Atomic rms distributions about the averaged structure (in Å) for the α-carbon atoms of the 18 refined distance geometry structures of PLA_2 in the ternary complex, as a function of the residue number.

it was deduced that Lys^{56} interacts with the headgroup of substrates and inhibitors (Noel et al., 1991; Lugtigheid et al., 1993). The identity of the other upfield ^{15}N signal at 7.43/33.4 ppm is not yet clear; it does not originate from Arg^{53}, which is also thought to have interactions with substrates and inhibitors. The ^{15}N-HSQC spectrum of the R53M PLA_2 mutant is in the upfield ^{15}N part identical to the HSQC spectrum of the wild-type enzyme (B. van den Berg, unpublished results).

Resonance and NOE assignments of PLA_2 in the ternary complex

Using gel filtration chromatography, the total size of the ternary complex was found to be the same as for the enzyme–micelle complex and estimated to be 40 ± 5 kDa. This value is in accord with a previous estimate by Dekker et al. (1991) of 38 kDa, using time-resolved fluorescence spectroscopy. A molecular weight of 40 kDa is consistent with a composition of the complex of either one protein molecule and 60 DPC monomers or two protein molecules and 30 DPC monomers. Since we have never observed NOEs indicating dimer formation, the former interpretation (one protein per micelle) is more probable. Also, Jain et al. (1991) have shown that pancreatic PLA_2s are catalytically active as monomers on bilayer vesicles. Despite the large size of the complex, the quality of the triple-resonance HNCO, HNCA, HNCOCA and HCACO spectra is still acceptable. This can be seen from Fig. 3, where examples of selected ^{15}N planes from the HNCO, HNCA and HNCOCA spectra are shown. In the HNCOCA spectrum circa 90% of the resonances are present, whereas the HNCA spectrum contains 65% of the (weaker) interresidual connectivities. From the amide proton linewidths in the HMQC-J spectrum a T_2 of circa 16 ms was estimated, which yields a correlation time of approximately 12 ns, corresponding to an apparent molecular weight of 25–30 kDa for the enzyme in the ternary complex. This accounts for the good quality of the spectra and indicates that the protein has a relatively high mobility on the micellar surface. A similar observation was made by Lauterwein et al. (1979) for the case of mellitin complexed to DPC micelles. The resolution of the spectra is still sufficient to assign more than 85% of the backbone resonances. In the middle of both large central helices several correlations in the triple-resonance spectra were very weak, and in a number of cases even absent. Assignment problems were also encountered in the surface loop between residues Cys^{61} and Tyr^{69}, where the correlations for a number of backbone resonances were totally missing. In these regions we had to rely on the

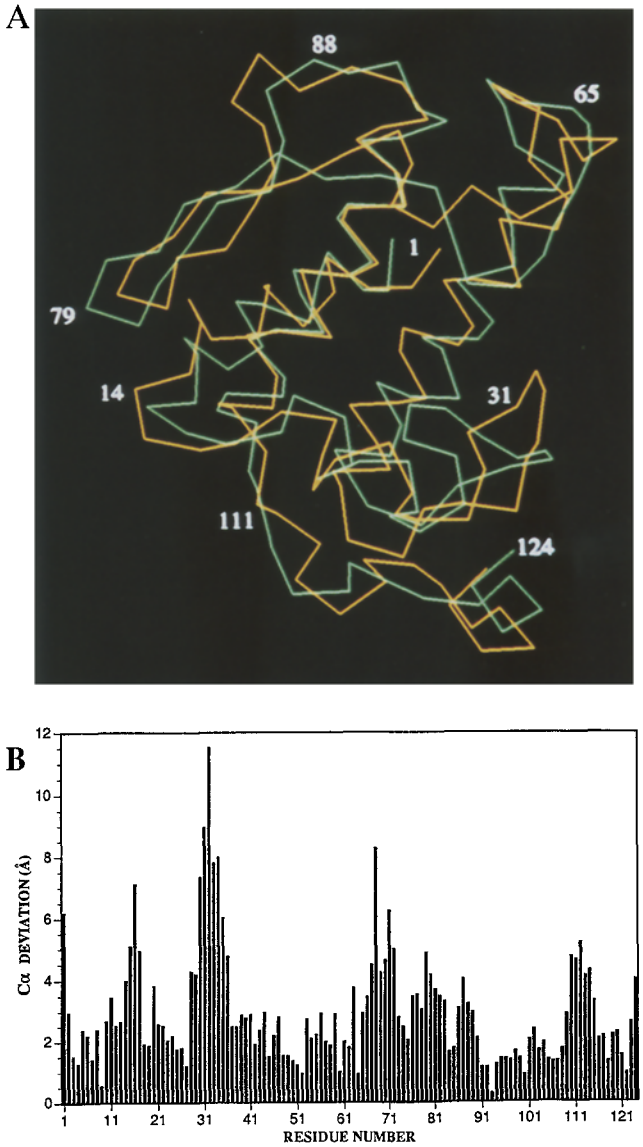

Fig. 8. (A) Best fit superposition of the C^{α} atoms of the restrained minimized averaged NMR structures of PLA_2 free in solution (orange) and in the ternary complex (green). The positions of some residues are indicated. (B) Deviations in C^{α} positions between the NMR structures of the enzyme free in solution and in the ternary complex, shown as a function of the residue number.

heteronuclear 3D TOCSY and NOESY spectra to complete the sequential assignments.

After assignment of the backbone resonances, the side-chain assignments for many (long-chain) spin systems were readily obtained from the HCCH-TOCSY spectra. However, for several AMX spin systems the assignments of the side chains could only be obtained from 3D heteronuclear NOESY spectra. Most of these problematic spin systems are found in the middle regions of the large central helices, as was also the case for the backbone resonances, and in the N-terminal α-helix. In contrast, both backbone and side-chain resonances for the residues in the C-terminal part of PLA_2 (residues Pro^{110} to Cys^{124}) are intense and could be easily assigned. The resonance assignments for the aromatic side chains were obtained by comparison with the assignments of the free enzyme, and from the observation of intra- and interresidual NOE patterns in heteronuclear 3D NOESY spectra. Stereospecific assignments for the prochiral methyl groups of valine and leucine residues could be obtained for all residues of PLA_2 in the ternary complex. Most side chain δ-NH_2 resonances of asparagine residues were assigned, except those of Asn^{67}, Asn^{88} and Asn^{97}, as well as the ε-NH_2 resonances of Gln^4. The ε-NH resonances of the arginine residues could be assigned, but no assignments were obtained for the η_1 and η_2 $NH_{(2)}$ resonances of the arginines and the ζ (NH_3^+) resonances of lysines. At the end of the procedure more than 95% of the ^1H, ^{13}C and ^{15}N resonances of PLA_2 present in the ternary complex were assigned (the table with assignments is available as supplementary material).

The 3D time-shared [^{15}N,^{13}C]-NOESY spectrum is of sufficient quality to enable extraction of a large number of NOEs. This is illustrated in Fig. 4, where selected ^1H-^{13}C cross sections are shown of the ^{13}C part of the time-shared NOESY spectrum of PLA_2 in the ternary complex. The distribution of all NOEs and of the long-range NOEs is shown in Fig. 5. The final structures were calculated on the basis of 1792 approximate distance constraints, including 337 long-range ones, which is on average 15 constraints per residue.

The final structures

For PLA_2 in the ternary complex, 35 distance geometry structures were calculated. These structures were analysed for the presence of chiral, dihedral and distance constraint violations, which yielded a final set of 28 distance geometry structures. After refinement of these structures, distance and dihedral violations were acceptable (1–5 distance violations larger than 0.5 Å, none larger than 0.7 Å; 4–8 torsion angle violations larger than 5°). The total energies and the violation energies of the refined structures were analysed. The structures with high total energies and violation energies were discarded, which left a final set of 18 refined distance geometry conformers. The superposition of the backbone (N, C^α, CO) atoms of these conformers is shown in Fig. 6. It is clear that the structures are well defined for large parts of the protein. The average rms difference between the 18 conformers with respect to the average structure is 0.89 ± 0.09 Å for the backbone atoms and 1.35 ± 0.10 Å for all atoms. If the disordered surface loop running from residues 62 through 72 is not taken into account, the rms difference values are 0.75 ± 0.09 Å for the backbone atoms and 1.14 ± 0.10 Å for all atoms. The 18 refined structures exhibit on average three distance violations larger than 0.5 Å (largest: 0.66 Å) and seven ϕ dihedral angle violations larger than 5° (largest: 35°). The stereochemical quality of the structures was checked with the program PRO-

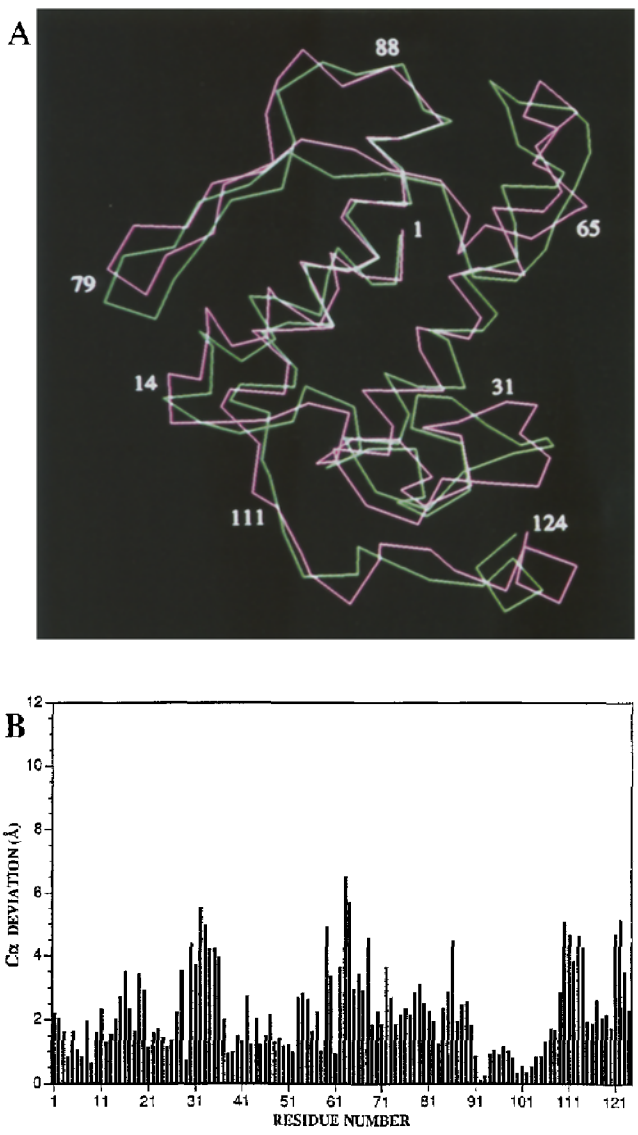

Fig. 9. (A) Best fit superposition of the C^α atoms of the restrained minimized averaged NMR structure of PLA_2 in the ternary complex (green) and the X-ray structure (purple). The positions of some residues are indicated. (B) Differences in C^α positions that occur in the ternary complex and the crystal structure, plotted as a function of the residue number. The X-ray structure is that of Finzel et al. (1991).

CHECK (Morris et al., 1992). All structures, as well as the energy minimized averaged structure, show reasonably good stereochemistry. Classifications range from 2 to 3 for the criteria of χ^1 and H-bond standard deviation. For the criterion of ϕ/ψ distribution, a few structures have a classification of 4 (Morris et al., 1992), with 52–55% of the residues present in the core regions of the Ramachandran plot. A probable reason for the somewhat lower stereochemical quality of the main chain is that relatively few dihedral angles could be obtained from the ^{15}N-HMQC-J spectrum due to the molecular size of the ternary complex. The proline and glycine residues are all present within the favoured regions with respect to their ϕ/ψ distribution (Morris et al., 1992).

To give an impression of the precision of the structure along the polypeptide chain, in Fig. 7 the α-carbon rms deviations of the ensemble of structures with respect to the averaged coordinates are shown as a function of the residue number. The largest rms deviations are found in the calcium-binding loop, the surface loop running from Lys^{62} through Ser^{72}, and the C-terminus (up from residue Asp^{119}). The positional variation of the calcium-binding loop arises during the refinement procedure. In the distance geometry structures, the position of the calcium loop is much better defined. The poor definition of the surface loop up to Pro^{68} is a reflection of the small number of NOE contacts present between this loop and the rest of the protein (Fig. 5). In the C-terminal region many NOE contacts are found, but most of these are sequential or medium-range. This preserves secondary structure, but it allows considerable conformational freedom for this part of the protein.

The structure of PLA_2 in the ternary complex: Comparison with the solution structure

The average rms difference between the PLA_2 conformers and the average structure is larger for the ternary complex than for the free enzyme (0.89 Å for the ternary complex and 0.68 Å for the free enzyme; Van den Berg et al., manuscript submitted for publication). This is due to the lower quality of the spectra of the complex and the consequently lower number of long-range NOEs (337 for the complex and 549 for the free enzyme).

The secondary structure of PLA_2 in the ternary complex is very similar to that in the free enzyme. However, considerable differences exist between the tertiary structures in both states of the enzyme, as is evident upon inspection of Fig. 8. The overall rms differences between both structures are as large as 3.5 Å for the backbone atoms and 4.0 Å for all atoms. These large rms deviations are mainly caused by differences in the positions of surface loops and turns in both states of the enzyme.

An important structural difference between the free enzyme and the enzyme in the ternary complex is located at the beginning of the N-terminal α-helix. Free in solution, the residues Ala^1, Leu^2 and Trp^3 have a non-α-helical, disordered conformation. The α-amino group of Ala^1 is pointing towards the solvent; its protons are in fast exchange with the solvent and therefore not visible in the spectra. In contrast, in the ternary complex the resonance of the α-amino group is clearly visible in all spectra. This suggests a buried position of the α-amino group in the interior of the protein. The structure of PLA_2 in the ternary complex indeed confirms that Ala^1, Leu^2 and Trp^3 are present in an α-helical conformation, with the α-amino group shielded from the solvent in a well-defined position. In the ternary complex 13 long-range contacts could be assigned for Ala^1 (Figs. 4 and 5), as opposed to only one long-range contact in the free protein.

The residues Ala^1, Leu^2 and Trp^3 show numerous NOEs with residues Tyr^{69}, Thr^{70}, Ser^{72} and Tyr^{73}. These interactions are caused by the inward movement of the N-terminal region and the surface loop around residues Tyr^{69} and Thr^{70}. The inward movement of the loop is the result of the interaction between the Tyr^{69} hydroxyl and the *sn*-3-phosphate of the inhibitor (Dijkstra et al., 1981, 1983; Kuipers et al., 1990a). Free in solution Tyr^{69} and Thr^{70} do not occupy an inward position. Furthermore, in the complex there is a displacement of the Trp^3 aromatic ring towards Ala^1, caused by the interaction of Trp^3 with the lipid micelle (Kuipers et al., 1990b).

The hairpin structure involving residues Tyr^{25} and Cys^{29} is quite evident in the ternary complex, but totally absent in the structure of free PLA_2. The remaining part of the calcium-binding loop (from Cys^{27} to Pro^{37}) has also a quite different conformation in both states of the enzyme, as is clear from Fig. 8. In solution the loop has a tilted position and seems much more exposed to the solvent. In the ternary complex the calcium loop has a conformation resembling that in the X-ray structure, as will be discussed later.

The surface loop running from Lys^{62} through Ser^{72} has significantly different conformations in the free enzyme and in the ternary complex. In both cases the loop seems to have a large degree of conformational freedom (up to residue Pro^{68}), as can be deduced from the intense cross peaks of several residues in this region in TOCSY-type spectra, and from the weak correlations of the same residues in the NOESY spectra. In the ternary complex the surface loop is pointing inwards, consistent with the interaction of Tyr^{69} with the phosphate group of the inhibitor. The inward position of the Tyr^{69} aromatic ring is evidenced in our spectra by the observation of NOEs to the ring of Tyr^{52}, and especially by the presence of several NOEs to Leu^{31}, which is part of the calcium-binding loop. It is well established that both the calcium ion and the Tyr^{69} hydroxyl have interactions with the phosphate group (Scott et al., 1990). The inward position of the loop is responsible for large differences in chemical shifts of this region in the ternary complex compared to the free

enzyme. In addition, residues in the loop interact with the lipid micelle, also contributing to the chemical shift differences observed in both environments (Kuipers et al., 1989).

The β-sheet from Ser^{74} through Asn^{85} is clearly present in the ternary complex. The position of the sheet, however, is quite different in the complex compared to PLA_2 free in solution. The turn Asn^{85}-Asn^{88}, following the β-sheet, is not clearly present in the ternary complex. From Ala^{90} up to the C-terminal residue Cys^{124}, the NMR structures of PLA_2 free in solution and in the ternary complex are similar.

Comparison of the NMR structure of PLA_2 in the ternary complex with the crystal structure

The crystal structure of PLA_2 determined by Finzel et al. (1991) will be referred to as 'the crystal structure'. In comparing this with the NMR structure, the emphasis will be on the regions that are likely to be important for the mechanism of action of PLA_2, i.e., the N-terminus, the calcium-binding loop and the surface loop. The deviations between the NMR structure of the ternary complex and the crystal structure are evident upon inspection of Fig. 9. The overall rms difference between the structure of the ternary complex and the crystal structure is 2.5 Å for the backbone atoms and 3.4 Å for all atoms. Both the position and the conformation of the N-terminal region and the calcium-binding loop are similar in the NMR structure of PLA_2 in the ternary complex and in the crystal structure.

The region of the surface loop running from Lys^{62} through Pro^{68} is not well defined in our structures, as is evident from Fig. 7. The poor definition of this segment arises from the absence of (long-range) NOEs, presumably due to a high flexibility in this region. However, on average it is clear from Fig. 9 that the loop region from residues 66 through 72 resembles fairly well the crystal structure. In both cases the loop is pointing inwards, due to the interaction of Tyr^{69} with the inhibitor.

The structure of PLA_2 in the ternary complex: Relation to interfacial activation

From biochemical and crystallographic studies it appears that a fixed position of the α-amino group in the interior of the protein is essential for interfacial binding and catalytic activity (Verheij et al., 1981; Dijkstra et al., 1982,1984). The high-resolution structure of free PLA_2 shows that residue Ala^1 is disordered, and that the hydrogen bonds linking the α-amino group to the active site are absent (Van den Berg et al., manuscript submitted for publication). The position of the α-amino group in the ternary complex is totally different from that in the free enzyme. In the complex, the α-amino group is shifted towards the interior of the protein, which results in much smaller distances from the α-amino group to the active-site residues Tyr^{52} and Asp^{99} compared to the free enzyme. For example, in the ternary complex the distances between the α-amino group and residues Tyr^{52} and Asp^{99} are between 3 and 4 Å. In contrast, in the free enzyme these distances range from 8 to 11 Å, excluding the formation of hydrogen bonds. In the crystal structure the contacts between the α-amino group and the active site are mediated by a water molecule. The hydrogen bond(s) between Ala^1 and Asp^{99} might be very important to provide a rigid, optimal conformation of the N-terminus and the active-site residues.

The surface loop from residues Lys^{62} through Ser^{72} has a disordered conformation in free PLA_2. In the crystal structures of the bovine pancreatic proenzyme and the transaminated bovine pancreatic enzyme (which cannot form the hydrogen bonds between the α-amino group and the active site), the first three N-terminal residues and the surface loop are disordered (Dijkstra et al., 1982,1984). One might therefore expect that in the ternary complex both the N-terminal region and the surface loop have a better defined conformation than in the free enzyme. Whereas this is certainly true for the first three N-terminal residues, a large part of the surface loop still has a disordered structure in the ternary complex. Only the residues Tyr^{69}, Thr^{70}, Glu^{71} and Ser^{72} adopt a well-defined conformation (Fig. 7), due to interactions with the N-terminal region.

Conformation of the inhibitor in the ternary complex

The structure of the inhibitor in the ensemble of conformers of PLA_2 in the ternary complex is shown in Fig. 10. The structure of the inhibitor in the active site resembles the one found in X-ray crystallographic studies (Thunnissen et al., 1990). For the alkyl chain attached to the *sn*-1 position, intermolecular contacts could only be assigned to Leu^{31}. In addition, the *sn*-1-methylene group has a contact to the His^{48} $C^{\varepsilon 1}$ proton. From Fig. 10 it can be inferred that the *sn*-1 chain protrudes from the protein into the lipid micelle. Except for residue Leu^{31}, only few interactions of the inhibitor with the rest of the protein are possible. This observation is supported by the crystal structure of the enzyme–inhibitor complex (Thunnissen et al., 1990). The sn-2-acyl chain is tightly bound in the hydrophobic binding pocket of the enzyme. This chain has multiple interactions with the aromatic residues Phe^5, Phe^{22} and Phe^{106}, as well as with Ile^9. The position of the *sn*-3 chain is determined by the interactions of the inhibitor phosphate group with the calcium ion and the hydroxyl group of Tyr^{69}. In addition, a hydrogen bond is likely to be present between the Lys^{56} NH_3^+ group and the *sn*-3-hydroxyl headgroup.

Conclusions

From the extensive crystallographic studies performed

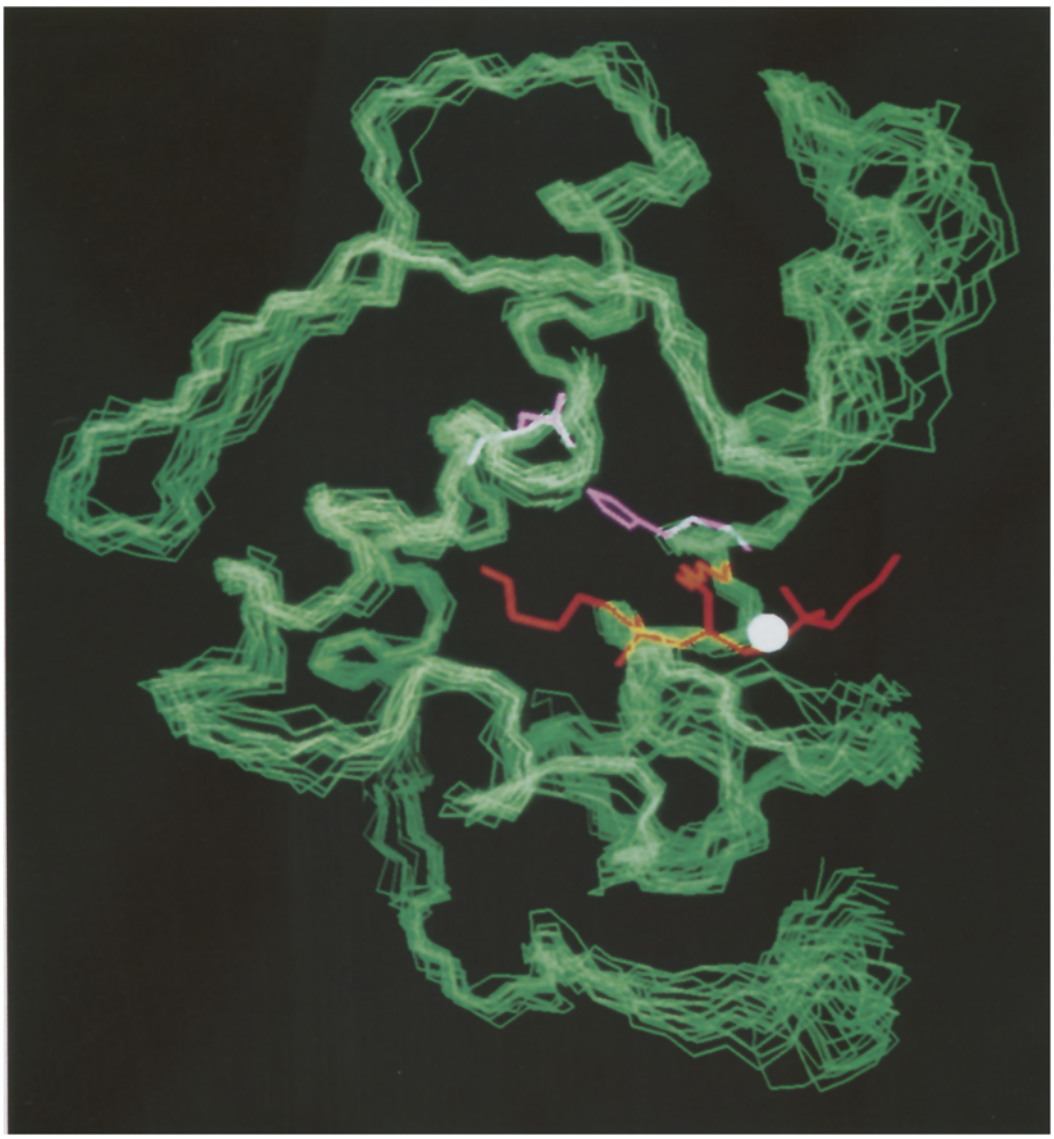

Fig. 10. Conformation of the phosphonate transition-state analogue in the active site of PLA_2 in the ternary complex. The backbone atoms (N, C^{α}, C') of the ensemble of enzyme conformers have been superimposed on the averaged minimized structure. Both active-site residues His^{48} and Asp^{99} are indicated in purple. The inhibitor molecule is shown in red; the calcium ion is shown as a white sphere.

on various PLA_2s, it was concluded that conformational changes do not play a role in the interfacial activation process of these enzymes (Scott and Sigler, 1994). In contrast, comparison of the solution structures of free PLA_2 and that in the ternary complex indicates that conformational changes play a role in the mechanism of interfacial activation of this lipolytic enzyme. We propose that an essential feature for high catalytic activity of the enzyme is an α-helical conformation of the first N-terminal residues, with the α-amino group occupying a position buried inside the protein. This position of the α-amino group enables hydrogen bond formation between the α-amino group and the active-site residues. These hydrogen bonds render the active-site residues a rigid, catalytically optimal conformation, which is also observed in the crystal structure of the free enzyme. The conformation of the free enzyme as observed in the crystal structure could be the result of a preferential crystallization of one protein conformer, resembling the solution structure of the enzyme bound to a lipid aggregate.

Acknowledgements

We would like to thank Dr. M.H. Gelb for valuable information concerning the synthesis of the phosphonate inhibitor, and Ruud Cox for his help in determining the molecular weight of the ternary complex by gel filtration. Part of this research was carried out with financial support of the Bridge programme of the European Community under contract no. NBiot-0194 NL.

References

Bax, A., Clore, G.M., Driscoll, P.C., Gronenborn, A.M., Ikura, M. and Kay, L.E. (1990a) *J. Magn. Reson.*, **87**, 620–627.

Bax, A., Clore, G.M. and Gronenborn, A.M. (1990b) *J. Magn. Reson.*, **88**, 425–431.

Bax, A. and Ikura, M. (1991) *J. Biomol. NMR*, **1**, 99–104.

De Araujo, P.S., Rosseneu, M.Y., Kremer, J.M.H., Van Zoelen, E.J.J. and De Haas, G.H. (1979) *Biochemistry*, **18**, 580–586.

De Haas, G.H., Dijkman, R., Van Oort, M.G. and Verger, R. (1990) *Biochim. Biophys. Acta*, **1043**, 75–82.

Dekker, N., Peters, A.R., Slotboom, A.J., Boelens, R., Kaptein, R., Dijkman, R. and De Haas, G.H. (1991) *Eur. J. Biochem.*, **199**, 601–607.

Dijkstra, B.W., Kalk, K.H., Hol, W.G.J. and Drenth, J. (1981) *J. Mol. Biol.*, **147**, 97–123.

Dijkstra, B.W., Van Nes, G.J.H., Kalk, K.H., Brandenburg, N.P., Hol, W.G.J. and Drenth, J. (1982) *Acta Crystallogr.*, **B38**, 793–799.

Dijkstra, B.W., Renetseder, R., Kalk, K.H., Hol, W.G.J. and Drenth, J. (1983) *J. Mol. Biol.*, **168**, 163–179.

Dijkstra, B.W., Kalk, K.H., Drenth, J., De Haas, G.H., Egmond, M.R. and Slotboom, A.J. (1984) *Biochemistry*, **23**, 2759–2766.

Finzel, B.C., Ohlendorf, D.H., Weber, P.C. and Salemme, F.R. (1991) *Acta Crystallogr.*, **B47**, 558–559.

Havel, T.F. (1991) *Prog. Biophys. Mol. Biol.*, **56**, 43–78.

Ikura, M., Kay, L.E. and Bax, A. (1990a) *Biochemistry*, **29**, 4659–4667.

Ikura, M., Kay, L.E., Tschudin, R. and Bax, A. (1990b) *J. Magn. Reson.*, **86**, 204–209.

Irvine, R.F. (1982) *Biochem. J.*, **204**, 3–16.

Jain, M.K., Ranadive, G., Yu, B.-Z. and Verheij, H.M. (1991) *Biochemistry*, **30**, 7330–7340.

Kay, L.E. and Bax, A. (1989) *J. Magn. Reson.*, **86**, 110–126.

Kay, L.E., Ikura, M., Tschudin, R. and Bax, A. (1990) *J. Magn. Reson.*, **89**, 496–514.

Kuipers, O.P., Thunnissen, M.M.G.M., De Geus, P., Dijkstra, B.W., Drenth, J., Verheij, H.M. and De Haas, G.H. (1989) *Science*, **244**, 82–85.

Kuipers, O.P., Dekker, N., Verheij, H.M. and De Haas, G.H. (1990a) *Biochemistry*, **29**, 6094–6102.

Kuipers, O.P., Vincent, M., Brochon, J.-C., Verheij, H.M., De Haas, G.H. and Gallay, J. (1990b) *Time Res. Laser Spectrosc. II*, **1204**, 100–111.

Lauterwein, J., Bösch, C., Brown, L.R. and Wüthrich, K. (1979) *Biochim. Biophys. Acta*, **556**, 244–264.

Lugtigheid, R.B., Nicolaes, G.A.F., Veldhuizen, E.J.A., Slotboom, A.J., Verheij, H.M. and De Haas, G.H. (1993) *Eur. J. Biochem.*, **216**, 519–525.

Morris, A.L., MacArthur, W.M., Hutchinson, E.G. and Thornton, J.M. (1992) *Proteins*, **12**, 345–364.

Noel, J.P., Bingman, C.A., Deng, T., Dupureur, C.M., Hamilton, K.J., Jang, R.T., Kwak, J.-G., Sekhardu, C., Sundaralingam, M. and Tsai, M.-D. (1991) *Biochemistry*, **30**, 11801–11811.

Pardi, A., Billeter, M. and Wüthrich, K. (1984) *J. Mol. Biol.*, **180**, 741–747.

Pascal, S.M., Muhandiram, D.R., Yamazaki, T., Forman-Kay, J.D. and Kay, L.E. (1994) *J. Magn. Reson. Ser. B*, **103**, 197–201.

Peters, A.R., Dekker, N., Van den Berg, L., Boelens, R., Kaptein, R., Slotboom, A.J. and De Haas, G.H. (1992a) *Biochemistry*, **31**, 10024–10030.

Peters, A.R., Dekker, N., Van den Berg, L., Boelens, R., Slotboom, A.J., De Haas, G.H. and Kaptein, R. (1992b) *Biochimie*, **74**, 859–866.

Powers, R., Garrett, D.S., March, C.J., Frieden, E.A., Gronenborn, A.M. and Clore, G.M. (1993) *Biochemistry*, **32**, 6744–6762.

Ransac, S., Rivière, C., Soulié, J.M., Gancet, C., Verger, R. and De Haas, G.H. (1990) *Biochim. Biophys. Acta*, **1043**, 57–66.

Scott, D.L., White, S.P., Otwinowski, Z., Yuan, W., Gelb, M.H. and Sigler, P.B. (1990) *Science*, **250**, 1541–1546.

Scott, D.L. and Sigler, P.B. (1994) *Adv. Protein Chem.*, **45**, 53–88.

Seilhamer, J.J., Pruzanski, W., Vadas, P., Plant, S., Millar, J.A., Kloss, J. and Johnson, L.K. (1989) *J. Biol. Chem.*, **264**, 5335–5338.

Senn, H., Werner, B., Messerle, B., Weber, C., Tzaber, R. and Wüthrich, K. (1989) *FEBS Lett.*, **249**, 113–118.

Thunnissen, M.M.G.M., Ab, E., Kalk, K.H., Drenth, J., Dijkstra, B.W., Kuipers, O.P., Dijkman, R., De Haas, G.H. and Verheij, H.M. (1990) *Nature*, **347**, 689–691.

Van den Berg, L. (1994) Ph.D. Thesis, Utrecht University, Utrecht.

Van den Bosch, H. (1980) *Biochim. Biophys. Acta*, **604**, 191–246.

Verheij, H.M., Volwerk, J.J., Jansen, E.J., Puyk, W.C., Dijkstra, B.W., Drenth, J. and De Haas, G.H. (1980) *Biochemistry*, **19**, 743–750.

Verheij, H.M., Egmond, M.R. and De Haas, G.H. (1981) *Biochemistry*, **20**, 94–99.

Verger, R. and De Haas, G.H. (1976) *Annu. Rev. Biophys. Bioeng.*, **5**, 77–117.

Vis, H., Boelens, R., Mariani, M., Stroop, R., Vorgias, C.E., Wilson, K.S. and Kaptein, R. (1994) *Biochemistry*, **33**, 14858–14870.

Waite, M. (1987) In *Handbook of Lipid Research*, Vol. 5 (Ed., Hanahan, D.J.) Plenum Press, New York, NY, pp. 211–240.

Yu, L. and Dennis, E.A. (1991) *Proc. Natl. Acad. Sci. USA*, **88**, 9325–9329.

Yuan, W. and Gelb, M.H. (1988) *J. Am. Chem. Soc.*, **110**, 2665–2666.